Thermoelectric Polymers

DOI: 10.1002/anie.201408431

Polymer Composites for Thermoelectric Applications

*Brendan T. McGrail, Alp Sehirlioglu, and Emily Pentzer**

composites · conjugation · polymer–particle interfaces · polymers · thermoelectric effect

This review covers recently reported polymer composites that show a thermoelectric (TE) effect and thus have potential application as thermoelectric generators and Peltier coolers. The growing need for CO_2-minimizing energy sources and thermal management systems makes the development of new TE materials a key challenge for researchers across many fields, particularly in light of the scarcity or toxicity of traditional inorganic TE materials based on Te and Pb. Recent reports of composites with inorganic and organic additives in conjugated and insulating polymer matrices are covered, as well as the techniques needed to fully characterize their TE properties.

1. Introduction

1.1. Thermoelectric Materials and Devices

The management and interconversion of energy is of the utmost importance as the world is increasingly industrialized and the population grows. Indeed, researchers are working to transform different sources of energy, including sunlight, wind, and nuclear power, into usable current and store this energy safely and efficiently.[1] As over half of the heat generated currently dissipates unused into the atmosphere and extensive energy input is required to cool machines and buildings, one of the most attractive areas for energy management centers on the utilization and manipulation of thermal energy (i.e., heat).[2] Specifically, thermoelectric (TE) generators harvest current from a heat source and Peltier coolers remove heat upon application of a current. To date, TE devices have been relegated to niche applications, such as space and industrial power plant technologies because of their relatively low efficiencies and high costs.[3] Continued improvements in thermoelectric material properties and device design will allow for efficient thermal management under a number of different operating conditions.

The fundamental unit of a TE device is a unicouple: legs of n-type and p-type materials connected through electrodes (Figure 1 A). Connecting tens to hundreds of unicouples electrically in series and thermally in parallel forms a TE module—a functioning device (Figure 1 B).[4,5] Exposure of one side to a heat source or sink creates a temperature differential across the device, which leads to a voltage difference, causing charges to move from the hot end to the cold end of the material (i.e., the Seebeck effect). Properties of TE materials are quantified by the unit-less Figure of Merit [ZT, see Equation (1)], composed of electrical conductivity (σ, with charge carrier of electrons for n-type and holes for p-type materials), Seebeck coefficient (α, positive for p-type and negative for n-type), and thermal conductivity (κ).[4] The Seebeck coefficient, also called the thermopower, is the electrical potential difference generated per degree of

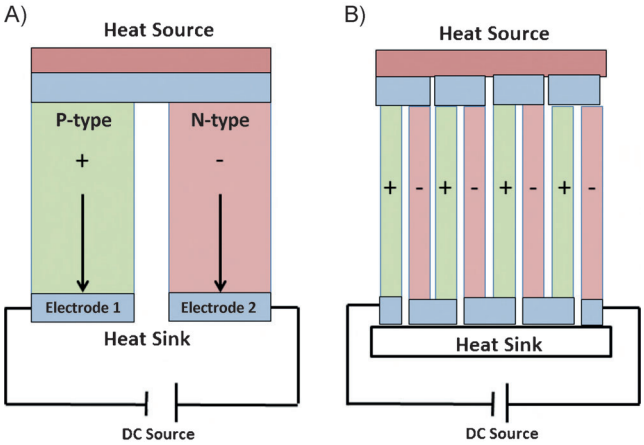

Figure 1. A) TE unicouple for Peltier cooling; B) TE module with multiple unicouples connected electrically in series and thermally in parallel.

[*] B. T. McGrail, Dr. E. Pentzer
Case Western Reserve University, Chemistry
10900 Euclid Ave, Cleveland, OH 44106 (USA)
E-mail: ebp24@case.edu
Dr. A. Sehirlioglu
Case Western Reserve University, Materials Science and Engineering
10900 Euclid Ave, Cleveland, OH 44106 (USA)

temperature difference ($\Delta V/\Delta T$). Under most conditions, σ, α, and κ are interdependent, with increased σ giving decreased α and increased κ.[4] Thus, optimization of one factor can have a detrimental effect on another. Values of ZT greater than one are needed for device efficiency over 10%.[6] Moreover, device-specific issues, such as difference in thermal expansion coefficient of each leg and contact resistance between materials and electrodes must be accounted for and overcome, as recently demonstrated for TE generators in the passenger vehicles BMW X6 and Lincoln MKT.[7] Methods for addressing these issues can be found elsewhere.[8,9]

$$ZT = T\frac{\sigma\alpha^2}{\kappa} \quad (1)$$

Industrial applications for TE materials, such as heat recovery from combustion engines and power stations, utilize ΔT values (temperature difference between two sides of the device) of 200–1000 °C.[3] Alloyed inorganic metals, such as PbSeTe/PbTe and Bi_2Te_3/Sb_2Te_3, show promise in these applications as a result of good thermal stability at the operating temperature, and ease of doping to tune electronic character and obtain both n-type and p-type materials.[10,11] ZT of these materials have been improved by the introduction of precipitates and rattlers, by processing of superlattices, and by accessing thermodynamically stable phase separation (during solidification, mechanochemical synthesis, hot pressing, spark plasma sintering, and microwave sintering).[12–15] These processing conditions create interfaces (grain and domain boundaries) which scatter phonons, decreasing κ without expense to σ, and improving ZT. As the scarcity and toxicity of the component metals is of concern, scalability and safety has been addressed by moving beyond Te- and Pb-based materials to silicon and transition-metal oxides.[16–18]

Devices composed of inorganic materials are generally heavy, cumbersome, and can have limited scalability because of the price of materials or processing techniques (e.g., manual assembly of devices); as such, replacing some inorganic materials with organic materials composed of abundant atoms (C, N, S, and H) is of great interest and facilitated by improved synthetic methodologies and processing conditions.[19–21] Organic polymers have good mechanical properties and can produce low cost and lightweight portable personal devices using scalable techniques, such as roll-to-roll and inkjet printing.[22] While most polymers are insulating, conjugated polymers are conductive because of charge delocalization across the polymer backbone, and show a correlated tradeoff between σ and α, as with inorganic materials, but tend to have extremely low thermal conductivities (0.1–1 $W\,m^{-1}K^{-1}$), electrical mobilities across a rather large range (10^{-8} to $10^4\,S\,cm^{-1}$), and absolute values of Seebeck coefficients ranging from 10–10^3 $\mu V\,K^{-1}$.[5,23] Thus, in characterizing organic TE materials, κ is at times ignored and the power factor ($PF = \sigma\alpha^2$) is reported, giving values for organic compounds that can be misleadingly low compared to inorganic materials. While definitive structure–property relationships have yet to be determined,[24] σ can be improved by organization and strong intermolecular interactions between conjugated polymer chains in the solid state (crystallization), which can provide boundaries that also lower κ (by phonon scattering).[25] Polymer-based TE devices will have operating temperatures below approximately 250 °C (assuming room temperature is T_{cold})[26] as a result of polymer melting and decomposition above around 300 °C,[27] and will find widespread use in lightweight and portable devices.

Brendan McGrail was born in Pittsburgh, Pennsylvania, US. After receiving his BSE in Polymer Science and Engineering from Case Western Reserve University (2009), he worked at W.L. Gore and Associates on projects integrating monomer synthesis, tribology, and surface analysis. He received his PhD in inorganic chemistry from the University of Notre Dame (2013) under Professor Peter Burns. He returned to CWRU to work on polymer nanocomposites with Professor Emily Pentzer in 2013, where his research focuses on polymer matrix nanocomposites with 2D nanomaterials for electronic applications.

Alp Sehirlioglu was born in Ankara, Turkey. He received his BS in Metallurigical and Materials Engineering from Middle East Technical University (1997), MS in Ceramic Engineering from Alfred University (2000), and PhD in Materials Science and Engineering from the University of Illinois Urbana Champaign (2005). He joined the faculty at Case Western Reserve University in the Department of Materials Science and Engineering in 2014. His research interests include energy conversion materials with focus on extreme environments, specifically piezoelectrics, thermoelectrics, and oxide-based heterointerfaces.

Emily Pentzer, a native of Bedford, Indiana, received a BS in chemistry from Butler University (2005) and PhD in organic chemistry from Northwestern University (2010) under the direction of Professor Sonbinh T. Nguyen. Emily then worked with Professor Todd Emrick in the Polymer Science and Engineering Department at UMass Amherst where she focused on the synthesis and assembly of electronically active materials for organic photovoltaic applications. Emily joined the faculty at Case Western Reserve University in the Department of Chemistry in 2013, with active research in organic synthesis toward materials with improved electronic properties.

1.2. Organic Polymers as Thermoelectric Materials

The TE properties of a number of conjugated polymers, including polyacetylene (PA),[28] polyaniline (PANI),[29,30] polypyrrole (PPy),[31] polycarbazoles,[32,33] polythiophenes,[34] and poly(phenylene vinylenes) (PPV),[35] have been evaluated (Table 1). To date, most work has focused on poly(3,4-ethylenedioxythiophene) (PEDOT),[36–40] though coordination polymers have shown some of the highest PFs.[41] One route to improve electrical conductivity in conjugated poly-

Table 1: Highest power factors reported for doped conjugated polymers.

Material	Structure	Dopant	σ [S cm^{-1}]	α [μV K^{-1}]	PF [W m^{-1} K^{-2}]	Ref.
PA		I_2	44250	14	2.7×10^{-4}	[28]
PANI	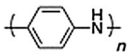	CSA^-	160	5	4×10^{-7}	[30]
PPy		PF_6^-	340	10.5	2×10^{-6}	[31]
Polycarbazole derivatives	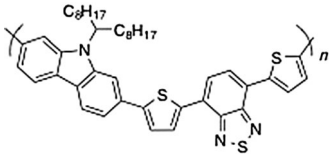	$FeCl_3$	160	34	1.9×10^{-5}	[33]
PPV derivatives	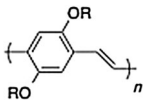	I_2	349	47	7.8×10^{-5}	[35]
PEDOT:PSS	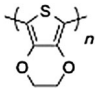	DMSO/EG	890	74	4.7×10^{-4}	[36]

Abbreviations: PA = polyacetylene, PANI = polyaniline, PPy = polypyrrole, PPV = poly(phenylene vinylene), PEDOT = poly(3,4-ethylenedioxythiophene), PSS = polystyrene sulfonate, CSA = camphor sulfonate, DMSO = dimethyl sulfoxide, EG = ethylene glycol.

mers is electrochemical or chemical doping to introduce extra charge carriers, such as polarons and dipolarons, and favor charge transfer along the polymer chains over hopping. Unfortunately, doping can also cause the Fermi level to move closer in energy to the conduction band, decreasing α. Moreover, a material can be n-type or p-type, depending on the identity of the dopant, and readers are directed to recent reviews that outline optimized TE properties of conjugated polymers.[42] The highest PFs for doped conjugated polymers are generally determined empirically,[4] and are shown in Table 1. Several recent reviews address polymer-based TE materials and their optimization, focusing on: fundamental physics such as carrier mobilities and interdependency of TE parameters and electronic aspects of the systems,[4,26] organic TE materials,[42] preparative aspects of composites,[5] and a survey of organic TE materials.[6]

This review focuses on recent reports of polymer composites for TE applications and the methods for their characterization as a route to identify and optimize promising materials. We briefly discuss polymer blends, then address conductive polymer matrices with inorganic TE materials, such as metal chalcogenides, noble metals, and carbon nanostructures. Insulating commodity polymer matrices for nanoparticles are then highlighted. Finally, methods to characterize σ, κ, and α are discussed, including special considerations for organic polymer composites. We conclude with a perspective and outlook for the future of organic composites as TE materials, highlighted by major challenges to overcome.

2. Thermoelectric Properties of Polymer Blends and Composites

One of the simplest and most cost-effective methods for modifying polymer properties is blending with small molecule, polymer, or nanoparticle additives. Many small molecules and simple inorganic salts are soluble in polymer matrices[43,44] and have been widely studied in electronic applications, including organic solar cells and field-effect transistors.[45,46] Composites are prepared by monomer polymerization in the presence of nanoparticles, in situ reduction of inorganic salts to form (nano)particles in the presence of a polymer, or solution blending of polymers and nanoparticles. Generally, homogeneous and uniform dispersion of nanoparticles in the polymer matrix give optimized properties,[47] and ligand exchange or covalent modification of nanoparticles can be used to ensure that the two components are miscible and optimize polymer–particle interactions.[48] Moreover, the polymer/nanoparticle or crystalline/amorphous polymer interfaces create boundaries that scatter phonons, thus ensuring low thermal conductivity.[49–51]

For TE applications, polymers can be insulating (polystyrene, PS) or conductive (polyaniline, PANI), and the nanoparticulate additives can be inorganic (e.g., Bi_2Te_3) or organic (e.g., C_{60} fullerene), with the only stipulation being that the conductive domains connect through the active area of the material.[52] Particles of a variety of sizes and aspect ratios can be used, including spheres, rods, and platelets, and the particle surface can facilitate polymer organization (crystallization) to improve σ. When both components have TE properties and are p-type or n-type, they work synergistically to improve ZT or, if of opposing carrier type, the blend can be p- or n-type depending on the relative ratio of the materials. Furthermore, the Fermi levels of two conductive

materials must be matched to minimize the energy barrier for charge carriers traveling between the two phases. As such, appropriate selection of materials, size, and shape of the particles, and polymer/particle interactions can be used to optimize *ZT*. A list of common p-type and n-type materials used in polymer composites is provided in Table 2; the TE properties of composites discussed herein are summarized in Table 3.

Table 2: Semiconductor materials commonly used for TE applications and their carrier types.

P-Type	N-Type
doped PEDOT	PEDOT
Bi_2Te_3[a]	Bi_2Te_3[a]
MoS_2 (bulk)	MoS_2 (single sheet)
polypyrrole (PPy)	perylene
graphene[b]	graphene[b]
graphene Oxide	tellurium
polythiophene	C_{60}
polyaniline (PANI)	SWCNT and MWCNT

[a] Bi_2Te_3 carrier type determined by the precise stoichiometry of atoms. [b] Graphene carrier type is dependent on the method of preparation and doping.

2.1. Polymer Blended with Polymers and Small Molecules

ZT of conjugated polymers have been optimized using polymer–polymer blends, with extensive success of a physical blend of poly(3,4-ethylenedioxythiophene) and poly(styrene sulfonate) (Table 1, PEDOT:PSS). Aqueous PEDOT:PSS suspensions are commercially available in various grades, and have found widespread use in photovoltaic and light-emitting-diode applications.[53] In the highly conductive form, PEDOT is oxidized (i.e., doped) and PSS provides charge balance. Solvents/additives with high boiling points have been used to selectively remove excess PSS and crystallize PEDOT, with work by Pipe and co-workers demonstrating the highest *ZT* (0.42) for a p-type organic system by adding 5 vol% DMSO to the PEDOT:PSS solution, thermally annealing the film, and immersing it in ethylene glycol (EG).[36] Heeger and co-workers blended a conductive polymer, PANI, with insulating PS or poly(methylmethacrylate)[54,55] to give PANI nanowires percolating the insulating matrix, even at low loading (<1 vol% PANI). Unfortunately, both α ($\approx 8.0\,\mu V\,K^{-1}$ at

Table 3: Optimized thermoelectric performance for polymer composites.

Matrix	Filler	Filler form	Loading [wt%]	σ [$S\,cm^{-1}$]	κ [$W\,m^{-1}\,K^{-1}$]	α [$\mu V\,K^{-1}$]	PF [$W\,m^{-1}\,K^{-2}$]	*ZT*	Ref.
Conductive polymers with polymer and small-molecule additives									
PS	PANI-HCl	blend	0.2	0.046	–	8	6.4×10^{-6}	–	[54]
PMMA	PANI-CSA	blend	0.091	10^{-3}	–	8	–	–	[55]
P3HT/P3HTT	F_4TCNQ	blend	1.2	2×10^{-4}	–	450	1.2×10^{-9}	1.4×10^{-5}	[56]
P(NDIOD)-T2	dihydrobenz-imidazoles	blend	9	0.004	–	−850	–	–	[58]
Conductive polymer matrices with particle additives									
PEDOT:PSS	PbTe	spherical	30	0.003	–	2500	1.45×10^{-6}	–	[59]
PEDOT:PSS	Te	nanowire	–	19	0.22	163	7×10^{-5}	0.1	[61]
PANI-HCl	Bi_2Te_3	nanowire	30	11.6	0.11	40	2.0×10^{-4}	0.004	[63]
PEDOT:PSS	$Bi_{0.5}Sb_{1.5}Te_5$	platelet	4.1	1295	–	16	3.2×10^{-5}	–	[64]
PANI-HCl	MoS_2	platelet	85	0.8	–	8	–	–	[70]
PPy	MoS_2	platelet	85	0.8	–	82	–	–	[71]
P3OT	Ag	spherical	6	–	–	1283	–	–	[74]
PEDOT:PSS	Au	spherical	0.01	241	–	27	1.8×10^{-5}	0.016	[75]
PEDOT:PSS	SWCNT	nanotube	35	400	–	23	2.4×10^{-5}	0.02	[79]
PEDOT:PSS	SWCNT	nanotube	85	4000	–	16	1.02×10^{-4}	0.03	[80]
PANI-$MeSO_3H$	SWCNT	nanotube	6.6	530	–	33	0.6×10^{-6}	–	[49]
PANI-HCl	MWCNT	nanotube	1	14	0.27	80	–	0.01	[82]
PANI-HCl	graphene	platelet	50	123	–	34	1.4×10^{-5}	–	[83]
PANI-HCl	graphene oxide	platelet	10	7.5	0.41	28	6.01×10^{-7}	4.86×10^{-4}	[85]
Insulating polymer matrices with particle additives									
PEO	MoS_2	platelet	72 [mol%]	0.1	–	1.5	–	–	[72]
PVOAc	SWCNT	nanotube	20	48	0.34	40	–	0.006	[84]
PVOAc/*meso*-tetra-(4-carboxyphenyl)-porphine)	MWCNT	nanotube	12	71.1	–	78	10^{-6}	–	[88]
PVOAC/sodium deoxycholate	MWCNT	nanotube	12	1.28	–	71	10^{-6}	–	[88]
PEI/sodium dodecyl benzenesulfonate	CNT	nanotube	20	8.4	–	100	8.4×10^{-6}	–	[89]
PVDF	few-layer graphene	platelet	80	170	–	17	5.2×10^{-7}	–	[91]

300 K) and σ ($\approx 10^{-3}$) were relatively low, giving PF of 6.4×10^{-6} W m^{-1} K^{-2}.

Katz and co-workers doped blends of P3HT and poly(3-hexylthiothiophene) (P3HTT) with the small molecule tetrafluorotetracyanoquinodimethane (F_4TCNQ, 1.2 wt %).[56] P3HTT pinned the LUMO while the low-lying HOMO of F_4TCNQ (−8.34 eV) dispersed the Fermi level, in line with previous theoretical reports for enhancing α.[57] Although PF and σ remained low ($\approx 10^{-9}$ W m^{-1} K^{-2} and 10^{-4} S cm^{-1}, respectively), α improved compared to P3HT (450 vs. 10 μV K^{-1}), suggesting that σ and α can be decoupled, and improvement in one is not at expense of the other. Most notable among blends of polymers and small molecules, Chabinyc and co-workers investigated the n-type polymer poly{*N*,*N*′-bis(2-octyl-dodecyl)-1,4,5,8-napthalenedicarboximide-2,6-diyl]-alt-5,5′-(2,2′-bithiophene)} (P(NDIOD-T2)) doped with dihydrobenzimidazole derivatives (9 wt % each, Figure 2 A–C); phase separation of the polymer and small molecule was observed by AFM, and small islands formed on the film surface (white areas in Figure 2 E and 2F).[58] These composites showed high n-type Seebeck coefficients (−850 ± 90 μV K^{-1}), but relatively low σ (0.004–0.008 S cm^{-1}). While these results are promising, most organic composites for TE applications are composed of polymer/nanoparticle blends, and will be the focus of the remainder of this Section.

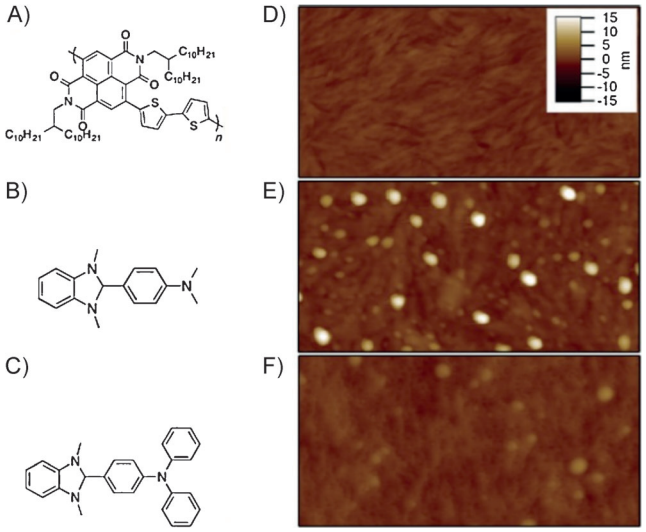

Figure 2. Structure of A) P(NDIOD-T2) polymer; B) dopant N-DMBI; C) dopant N-DPBI; atomic force micrographs of D) neat P(NDIOD-T2); E) P(NDIOD-T2) doped at 9 mol % with N-DMBI; F) and P-(NDIOD-T2) doped at 9 mol % with N-DPBI. Aggregates form on the top surface of the doped films. The images are 500 nm (vertical) by 1 μm (horizontal). Adapted from Ref. [58].

2.2. Polymer Composites with Semiconductor Nanomaterials

Some of the most promising polymer composites for TE applications incorporate inorganic particles that also show favorable bulk TE properties, specifically tellurium (Te), bismuth telluride (Bi_2Te_3), and lead telluride (PbTe). DMSO-treated composite films of PEDOT:PSS and spherical PbTe nanoparticles gave crystalline PEDOT nanowires decorated with nanoparticles.[59] At moderate PbTe loadings (21–43 wt %), a percolated nanoparticle network was not formed, yet α exceeded that of bulk Bi_2Te_3 ($\approx$2500 vs. 220 μV K^{-1})[60] and σ improved, resulting in an optimized PF of 1.45 μW m^{-1} K^{-2} at 30 wt % PbTe. Of note, PEDOT and PbTe have opposing charge carriers, and better matching of materials properties could further improve TE properties.

In another study, sodium tellurite was reduced in the presence of PEDOT:PSS or PEDOT:Tos (Tos = tosylate) to form TE nanowires ($\approx$4 by 84 nm) fully wetted with and well dispersed in the polymer matrix.[61] At the interface with Te NWs, PEDOT was highly ordered, and σ increased compared to bulk PEDOT:PSS, while κ remained low to give ZT values as high as 0.1, representing a distinct departure (improvement) from the simple mean-field model.[62] Similarly, electropolymerization of aniline in a suspension of Bi_2Te_3 NWs ($\approx 40 \times 900$ nm) gave ordered chains of PANI on the NWs.[63] A redshift in polaron absorption was observed, as well as doubling of σ and ZT relative to pristine polymer (11.6 S cm^{-1} and 0.004, and 7.8 S cm^{-1} and 0.002, respectively). Lin and co-workers showed $Bi_{0.5}Sb_{1.5}Te_3$ platelets (300–500 nm in diameter and 20 nm tall) prepared in the presence of PEDOT:PSS gave better particle dispersion, higher PF, and improved α over solution-blended composites at comparable particle loadings (4.1 wt %),[64] though measurements of the Hall effect showed poor interfacial charge-carrier transfer, which limited the performance. Perhaps surprisingly, a bilayer of Bi_2Te_3 particles (irregularly shaped, $\approx$0.5–3 μm) and PEDOT:PSS showed higher α and PF than any of these well-dispersed blends, though the reasons for this behavior are unclear.[65]

The relatively recent development of safe liquid-phase exfoliation of two-dimensional inorganic materials[66] has led to a surge of interest in chalcogenides composed of S or Se and transition metals. Of specific interest are molybdenum disulfide (MoS_2) nanosheets because of their inherent photothermoelectric effect.[67,68] PEDOT/MoS_2 nanocomposites were prepared, but the TE properties of this system were not explored;[69] however, Kanatzidis and co-workers prepared polymer-intercalated MoS_2 composites[70,71] with alternating platelet and polymer layers, as shown by powder X-ray diffraction. Composites were prepared by in situ polymerization of aniline or pyrrole to give low-MW polymer (polymer growth is stunted by platelets), or by blending insulating polyethylene and poly(ethylene oxide) (PE and PEO) with MoS_2.[72,73] All of these composites showed large σ ($\approx$0.1–0.8 S cm^{-1}) at room temperature, but relatively small α (1.5–8 μV K^{-1}), indicating that the platelets, and not the polymer, dominate charge transport. No systematic investigations to tune polymer–MoS_2 interactions for improved TE performance have been conducted, and recent single-platelet studies suggest that further attention in this area will be helpful.[67,68]

2.3. Polymer Composites with Noble-Metal (Au, Ag) Nanomaterials

In order to utilize nontoxic materials for TE applications, polymer composites with noble-metal nanoparticles have been investigated, though the performance has yet to rival that of other composites. Ag nanoparticles prepared by reduction of $AgClO_4$ in the presence of poly(3-octylthiophene) (P3OT) gave composites with large α (up to 1283 $\mu V K^{-1}$) and increased σ over P3OT (at 5 wt% Ag).[74] Wide-angle X-ray scattering (WAXS) showed better P3OT organization at the particle interface below the percolation threshold ($\approx$3 wt%), indicating interrupted polymer crystallization at higher loadings (Figure 3). Composites of PEDOT:PSS/AuNPs were prepared by in situ polymerization

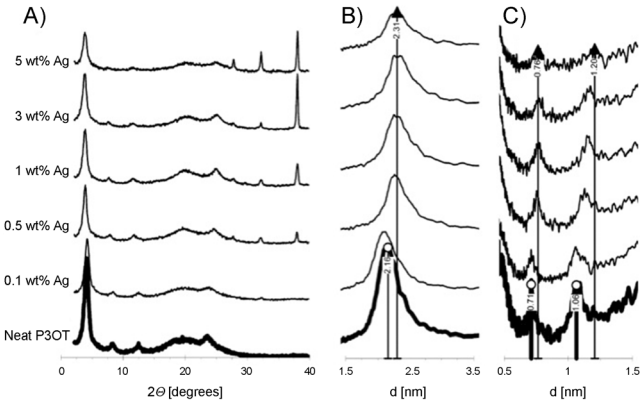

Figure 3. A) Full WAXS patterns of P3OT/Ag nanoparticle composites at different loadings of Ag (0, 0.1, 0.5, 1, 3, and 5 wt%); B,C) Details of WAXS of these composites plotted against calculated *d*-spacing. Center-of-gravity peak positions are marked for the highest silver concentration (top), as well as for the undoped polymer (bottom). Adapted from Ref. [74].

and showed small increases in PF and σ, and around 60% increase in ZT at extremely low AuNP loadings (10^{-3} wt%).[75] AuNPs with dodecanthiol ligands gave better properties than terthiophenethiol or poly(*N*-vinylpyrrolidone) ligands[75]—a surprising observation, given that the insulating and hydrophobic nature of the alkyl ligands should decrease miscibility with the water-soluble PEDOT:PSS. As such, further work to understand how ligand identity influences polymer/particle interactions and the relationship between α, σ, and κ is needed.

2.4. Polymer Composites with Carbon Nanomaterials

Over the past three decades, carbon nanomaterials and their polymer composites have received a great deal of attention for their outstanding thermal and electrical conductivity, mechanical strength, and low density.[76] Conjugated networks of sp^2-hybridized carbon atoms can be found as spherical (fullerenes), tubular (carbon nanotubes (CNTs)), and planar (graphene) geometries, exhibiting semiconducting or metallic characteristics depending on the precise C–C connectivity.[77] Modification of carbon nanomaterials with surfactants, polymers, or small molecules can overcome strong van der Waals interactions, prevent aggregation, and give dispersability in polymer matrices. For TE applications, polymer composites with CNTs have garnered the most attention, though the high cost and relatively restricted scalability of pristine CNTs can be limiting. Researchers must also overcome the high thermal conductivity and ambipolar transport of these materials (when metallic), which may place upper limits on their TE performance.

2.4.1. Conductive Polymer–CNT Composites

The overwhelming majority of carbon nanoparticle composites for TE applications utilize single- or multi-walled CNTs (SWCNTs or MWCNTs, respectively), which are generally semiconducting and p-type, though n-type and p-type SWCNTs have been used to prepare a functioning device.[78] Composites formed from Pickering emulsions of SWCNT-stabilized PEDOT:PSS showed improved TE properties relative to neat polymer, likely because of matrix–CNT electronic junctions. The method of film formation greatly influenced composite properties: monolithic samples prepared by drying at room temperature in a vacuum desiccator for 24 hours produced ZT less than half of that from samples heated to 80 °C for six hours, then dried in a vacuum desiccator for 24 hours (0.004 and 0.02, respectively).[79] Another study on similar composites showed little variance in PF based on SWCNT loading (0–85 wt%),[80] with gains in σ largely offset by decreased α (Figure 4). Thermal treatment, such as annealing, is one technique that could further improve performance by enhancing polymer crystallization and network formation.[81]

PANI-methanesulfonic acid and SWCNT or MWCNT composites showed strong polymer-filler interactions, with

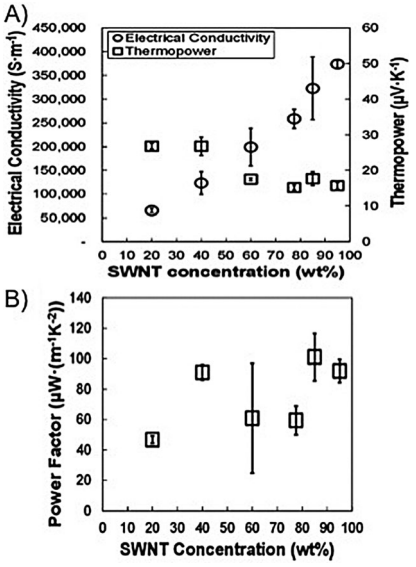

Figure 4. A) Electrical conductivity (left axis) and Seebeck coefficient (right axis) and B) power factor as a function of SWCNT loading for PEDOT:PSS composites. Adapted from Ref. [80].

PANI wrapped around the CNTs to give a continuous network of fibers. At 6.6 wt% SWCNT, α was 33 $\mu V K^{-1}$ and attempts to improve polymer/particle interactions by CNT oxidation decreased α to 12 $\mu V K^{-1}$.[49] Wang and co-workers used hydrochloric acid (HCl) in place of methanesulfonic acid to prepare PANI-HCl/MWCNT composites, and found that low loadings of CNT (< 1 wt%) gave optimized α (80 $\mu V K^{-1}$) and ZT (0.01).[82] As such, the identity of the dopant/counterion for PANI and the nanofiller affects the TE properties of composites, and optimized particle loading.

2.4.2. Conductive Polymer–Graphene Nanocomposites

Graphene, the one carbon atom thick planar sheet relative of the scrolled CNT, has received less attention as an additive to polymers for TE applications. Grinding and cold compression molding of PANI-HCl with graphene grown by chemical vapor deposition gave composites with α of 34 $\mu V K^{-1}$ and PF of 1.4×10^{-5} W $m^{-1} K^{-2}$ at 50 wt% loading.[83] Similar values were obtained for poly(vinyl acetate) (PVOAc)/SWCNT composites (Figure 5),[84] with TE properties optimized only when the carbon nanomaterials cluster/percolate the PANI matrix, indicating that particles, and not the polymer, dominates charge transport.

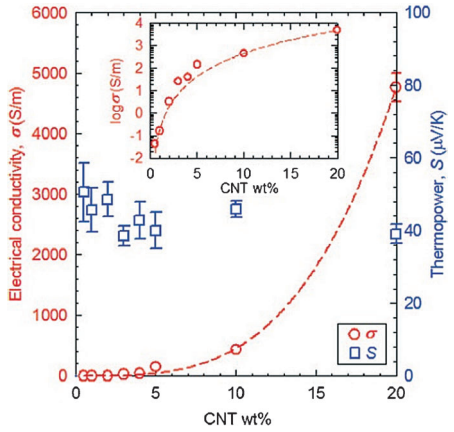

Figure 5. Electrical conductivity (left axis) and Seebeck coefficient (right axis) as a function of SWCNT loading in poly(vinyl acetate) (PVOAc). The inset shows a percolation threshold of about 5 wt% SWCNT. Adapted from Ref. [84].

To overcome aggregation of platelets as a result of van der Waals interactions, researchers chemically oxidize graphite to access graphene oxide (GO), crumpled (i.e., dispersible) sheets containing sp^2- and sp^3-hybridized carbon atoms and oxygen functionalities (epoxides and alcohols) throughout. While GO has much lower conductivity than graphene, it can be functionalized and dispersed in many polymers and chemically or thermally reduced to regain conductivity. Polymerization of aniline in the presence of GO resulted in PANI/GO composites with strong polymer/platelet interactions and ordering of the polymer at the interface, as determined by XPS and FTIR.[85] The composite showed σ of 7.5 S cm^{-1}, but ZT of only 4.86×10^{-4}.

2.5. Insulating Polymer–Nanoparticle Composites

In addition to the conjugated polymers that themselves behave as TE materials, insulating polymers can serve as a flexible and robust matrix for nanoparticles with TE properties. In contrast to rod-like conjugated polymers, coil-like insulating polymers with saturated backbones (i.e., not electronically active) can be processed using well-known techniques including electrospinning and extrusion. Furthermore, polyethylene, polypropylene, Nafion, and poly(vinylidene fluoride) (PVDF) can be readily prepared on a large scale using known chemistries, and can offer additional properties, such as stimuli-responsiveness.[86,87] Ideally, blending such polymers with TE nanoparticles would produce composites with the low thermal conductivity of the matrix, and σ and α dictated by the nanoparticulate additive. Thus, the composite will have TE properties when particles form a network, though the influence of wt% loading must be determined empirically.

In addition to MoS_2 single platelets incorporated in insulating PE and PEO,[72,73] SWCNTs and MWCNTs have been incorporated into insulating polymers as TE materials. Grunlan and co-workers prepared composites from SWCNT-stabilized Pickering emulsions of PVOAc/gum arabic in water, giving σ up to 48 S cm^{-1}, polymer-like low κ (0.34 W $m^{-1} K^{-1}$), σ increased with increased CNT loading, and an optimized ZT of around 0.006.[84] As the matrix and SWCNTs began to segregate at about 10 wt%, σ improved slowly, while the Seebeck coefficient remained largely unchanged over all loadings tested ($\approx$ 40 $\mu V K^{-1}$, Figure 5). In other work, MWCNT/PVOAc composites were prepared using the molecules *meso*-tetra(4-carboxyphenyl)porphine (a semiconductor) and sodium deoxycholate (an insulator) as emulsion stabilizers for the MWCNTs, but no significant property enhancement was observed.[88] Polyethyleneimine (PEI) and CNTs blended in the presence of the emulsifier sodium dodecylbenzenesulfonate (SDBS) gave composites with α of 100 $\mu V K^{-1}$ and σ of 8.4 S cm^{-1}.[89] In this system of 40 wt% PEI, 20 wt% CNT, and 40 wt% SDBS, the CNTs provide a network for conducting charges and the insulating PEI matrix disrupts the thermal contact between the CNTs. Alternating layers of n-type and p-type MWCNTs and PVDF were prepared by melt blending and pressing to give fabric-like devices, which generated a potential of 28 mV with a 50 K temperature gradient at extremely high MWCNT loadings (95 wt%); values for σ, α, and κ were not given.[90] Solution-blended and drop-cast films of PVDF with up to 90 wt% few-layer graphene (FLG) platelets showed an optimized Seebeck coefficient and power factor of 17 $\mu V K^{-1}$ and 5.2×10^{-7} W $m^{-1} K^{-2}$, respectively, though FLG began to segregate to the film surface above 40 wt% loading.[91]

3. Characterization of TE Properties

As discussed in the introduction, the usefulness of TE materials is determined by the Figure of merit (ZT), composed of σ, α, and κ [see Equation (1)]. The increasing demand from the commercial community for better stand-

ardization of characterization has driven round-robin measurements and standards development.[92,93] We now turn our focus to the practical aspects of measuring the values relative to TE performance and sources of error in these measurements. Figure 6 shows an example of measured properties and

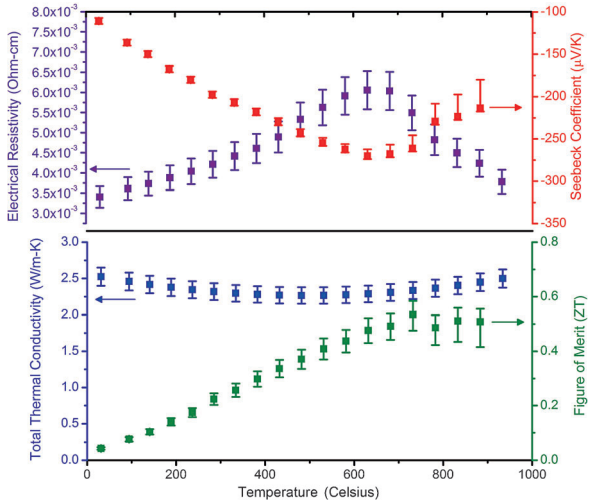

Figure 6. Measured σ, α, and κ, and calculated Figure of Merit as a function of temperature for a high-temperature thermoelectric (70/30 at% Si/Ge with 2 vol% WSi_2 and 2 at% P). Error bars are calculated based on a range of sources as discussed in this report and related references. Asymmetry in error bars of the Seebeck coefficient data at high temperatures is due to the cold-finger effect.

calculated ZT as a function of temperature with calculated error bars propagated from a variety of sources as will be introduced in this section. In addition to the characterization techniques discussed here, Hall measurements can be used to determine charge-carrier density and mobility.[94] Polymer composites for TE applications are still nascent compared to their inorganic counterparts, and their usefulness will ultimately be found in incorporation into devices, which requires matching p-type and n-type materials as well as taking into account thermal expansion coefficients and contact resistance with electrodes.[95,96]

3.1. Seebeck Coefficient

Accurate measurement of the Seebeck coefficient (α, $\Delta V/\Delta T$) is especially crucial to identifying good TE materials, as ZT is directly related to its square [Equation (1)]. Unfortunately, no standard exists for calibration of instrumentation for measuring α, especially for high-temperature materials. The most common technique for determining α utilizes a four-point-probe set-up and will be the focus here, though measurements under an AC field or external pressure have been used,[97,98] as well as the use of open-circuit voltage and short-circuit current.[99] Despite advantages of some of these techniques (e.g., elimination of the Peltier contribution in AC measurement set up) they generally require extensive sample preparation and are not conducive to polymer films. For low-temperature materials constantan, a Cu/Ni alloy with thermopower on par with polymer-based TE composites (−35 μV/°C), can be used for calibration. Four-point-probe techniques can measure both α and σ, and thus can be used to determine the PF ($\alpha^2\sigma$) of a material. Figure 7 A shows the design of the

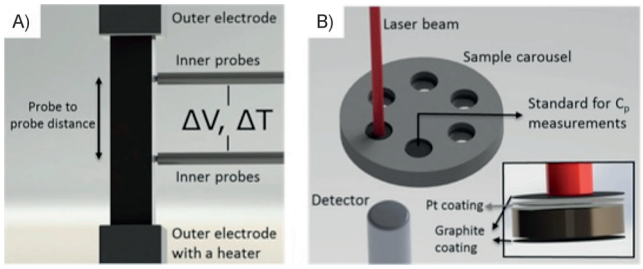

Figure 7. A) Schematic of four-point-probe geometry for measurement of Seebeck coefficient and electrical conductivity. The outer electrodes are conventional electrodes and measure ΔV, while the inner electrodes are thermocouples and can measure both ΔV and ΔT. B) Laser flash system showing irradiation of top of sample to measure thermal conductivity.

four-point-probe technique: regular electrodes are used as the outer contacts and provide Ohmic contacts, while the inner electrodes are thermocouples that measure both ΔV and ΔT. Notably, as the inner electrodes are TE materials themselves, their contribution to the measurements must be subtracted, taken as a wire Seebeck coefficient as described in Equation (2):

$$\alpha = -\frac{\Delta V}{\Delta T} + \alpha_{\text{wire}}(T) = -\frac{\sum x_i \sum y_i - N\sum x_i y_i}{(\sum x_i)^2 - N\sum x_i^2} + \alpha_{\text{wire}}(T) \qquad (2)$$

where the probe-to-probe temperature difference and voltage difference along the same wires are x_i and y_i, respectively. N is the sampling size and α_{wire} is the temperature-dependent Seebeck coefficient of the wires used to measure ΔV.

Seebeck coefficients are measured as a function of the temperature, and the experimental set up utilizes two heaters: one provides a constant temperature for the whole assembly and the measured σ and α are a function of this temperature, and the second heater creates ΔT across the material. The temperature distribution in a furnace can also be used to create ΔT across a material, but presents serious limitations and difficulties in characterization, and is limited at temperatures of interest for organic TE materials ($<300\,^\circ\text{C}$), requiring a length of the sample greater than may be practical. As such, a small heater is generally placed at one of the outer electrodes, in contact with the material, to produce ΔT across the length of the thermoelectric leg (i.e., the material).

By varying the temperature at one end of the thermoelectric leg using the secondary heater, ΔV and ΔT are measured using the inner probes. A quasi-steady-state measurement is realized either by measuring at discreet ΔT values or measuring as the internal heater is powered up and down continuously.[8,100] Thus, the $\Delta V - \Delta T$ slope can be used to calculate α. Offsets between the negative and positive

probe wires can be hard to control because of the presence of spurious voltages at $\Delta T = 0$, which may be inherent to the electronics and/or the variation of the temperature of the probes at the cold side, among other factors.[101] Quasi-steady-state conditions are favorable, as factors creating the offset can be ignored and a larger set of data points can be collected, decreasing statistical uncertainty of the measurement.[102] Determination of α requires measurement of the temperature from hot probe, temperature from cold probe, voltage drop measured with p-wires of the inner thermocouple probes, voltage drop measured with n-wires of the inner thermocouple probes, and the measurement of the cold end of the probes. Heating rates can significantly affect the accuracy of measurements because of staggered acquisition,[103] and the heating rate that creates ΔT should be kept low, around 1 °C per minute.

In performing four-point-probe measurements, the phase and morphology of the material is assumed to not change during temperature cycling, as this could introduce errors. Other sources of errors associated with the measurement of α are: 1) cold-finger effect, 2) wire Seebeck variation 3) precision of multimeters used for measurements, and 4) the statistical variation in calculation of Seebeck coefficients.[104] While some of these errors can be reduced by modifying the instrumentation (i.e., multimeters used), the impact of others can be reduced by modifying the measurement profile, for example, collecting a larger data set in quasi-steady-state profiles (see above). Certain errors can be measured and used as quality control of the instrumentation. Observed difference in α calculated using negative and positive wires of the thermocouple probes and comparison to a standard can determine the contamination of the probes, indicating the need to replace them. These measurements are relevant, provided the time between using the n- and p-wires is small.

Another source of error in determining α is the thermal boundary between the probe and the sample; a high-quality contact is necessary for accurate measurements. In the four-point-probe set-up, the inner probes are spring-loaded to provide good thermal contacts. Thus the sample and the thermocouple beads of the inner electrodes must be mechanically robust enough to handle the compressive forces and can be a few millimeters in size. The resulting temperature gradient between the surface of the material to be measured and the probe creates an error called the "cold-finger effect." This is a function of temperature, as the heat flow out of the sample increases with increasing temperature.[8,101,105] The cold-finger effect is larger on the probe closer to the heat source and creates an asymmetry in uncertainty, overestimating α.[104] In general, the operating temperature of organic thermoelectrics (< 300 °C)[4] makes these factors negligible, but they must be taken into account in the characterization of higher-temperature organic TE materials.[101]

3.2. Electrical Conductivity

Electrical conductivity (σ) can be determined using the same four-point-probe set-up discussed above. In this case, current is applied through the outer electrodes, and the voltage drop between the inner probes is measured, thereby eliminating problems associated with contact resistance on the outer electrodes. The measured resistance and geometric factors are used to calculate resistivity, so long as the material follows Ohms law. To prevent errors, the material of interest must be Ohmic over the experimental conditions.

The resistance of the material is calculated from the slope of V–I plots, and any deviation from the linearity can result in an error. Increasing the sampling size and measurement range can decrease the statistical error associated with the measurement of the slope, even for Ohmic materials. Measuring the voltage drop using both the n- and p-wires of the thermocouple is advised, and consistent results should be obtained for the two. Any difference can lead to errors in voltage measurement and indicate artifacts, such as deterioration of the thermocouple probes themselves. As inherent to TE materials, application of a current results in the Peltier effect, creating a temperature difference across the material, and can contribute to the overall heating of the sample through Joule heating. Errors originating from such factors can be decreased by applying current as pulses with millisecond pulse width and in a bipolar fashion. As in the measurement of α, errors in determining σ can be derived from the natural temperature profile in the furnace, and sufficient shielding around the measurement configuration is needed to keep ΔT minimized (< 1 °C), if not completely eliminated, during the measurement.

3.3. Thermal Conductivity

Although PF is determined by only σ and α, accurate determination of ZT necessitates measuring the thermal conductivity (κ). Because of the low thermal conductivity inherent to organic polymers, many researchers do not report a value, but a thorough evaluation of materials will include this measurement. Thermal conductivity is generally calculated by techniques that measure thermal diffusivity using Equation (3), and will be the focus here:

$$\kappa = \alpha C_p \rho \tag{3}$$

where κ, α, C_p and ρ are the heat conductivity, heat diffusivity, specific heat capacity, and density, respectively. As such, errors that originate from heat capacity and density measurements also contribute to the total error in thermal conductivity. Heat capacity can be measured in a laser flash system as well as externally in a differential scanning calorimeter (DSC).[106,107] The standard used in either technique needs to have heat capacity close to the expected value of the material under test to minimize errors.

Before discussing the details of the thermal diffusivity measurements, it is important to note that shape and size of the sample are very different for this technique compared to those used for the four-point-probe technique to measure α and σ; disc-shaped samples are used to determine κ, while dog-bone-shaped or rectangular samples are used to measure α and σ. Therefore, extra attention must be paid to sample preparation when working with materials that show aniso-

tropy originating from crystallographic or microstructure orientation, as this can influence the measured values. Non-uniform distribution of additives within samples or processing conditions can also produce anisotropy, and can derive from shear direction in tape casting (blade coating), piston direction in spark plasma sintering, or solidification direction in directionally solidified samples. Thus, to accurately define ZT of a material, which is relevant to device construction, all measurements should have the same directional relationship to the processing parameters and sample anisotropy. Therefore, attempts to measure properties on similarly shaped samples, specifically the measurement of α on disc-shaped materials are ongoing.[108] When reporting values of α, σ, and κ, researchers should note geometric anisotropy of the sample or demonstrate that no significant variation in the measurements is observed.

Thermal-conductivity measurements at low temperatures (i.e., below room temperature) do not suffer from errors associated with heat losses.[109] Hence, axial heat flow measurements provide accurate results and have the advantage of using bar/cylinder-shaped samples, similar to the shape used for measuring α and σ.[110] However, as the interest in higher-temperature organic materials increases, heat losses during the characterization of κ become relevant and similar to those observed in inorganic materials. Non-steady-state measurements, such as laser flash technique,[111] have advantages in dealing with thermal losses as a result of conduction, convection, and radiation. Most commercial systems for the measurement of thermal diffusivity solve the heat-flow equation with different thermal-boundary conditions and losses to explain deviations in the shape of the temperature–time curve, giving solutions applicable to the measured data. While it is generally advisable to keep the losses as small as possible, laser flash techniques can perform measurements even when losses are high, and currently available high-acquisition systems allow the accurate calculation of losses.[112,113]

Temperature–time curves are measured at the back surface of disc-shaped materials after initial irradiation of the front surface of the material. Thermal losses can be minimized by providing minimal contact to the sample using a ledge and use of a thin sample (<3 mm), as the latter decreases the measurement time and thus the thermal loss during measurement. Generally, the material to be measured is coated with two layers: one on the front (top) face to completely absorb the energy of the pulse, especially important for materials that are transparent/translucent to the wavelength of irradiation, and the second layer is a carbon-coat to provide uniform emissivity (Figure 7B). The absorption layer is critical for all measurement temperatures, as it provides uniform heating on the front surface, and is especially critical for high-temperature measurements, in which radiation losses are a factor. Additional sources of error originate from the measurement of the thickness and the thermal expansion of the material under testing.[114]

3.4. Measuring Thermoelectric Properties of Films

The techniques discussed above are widely applicable to and optimized for bulk materials and thus have limited use in the characterization of samples of small sizes and thin films; however, they serve as a starting point. Generally, samples of polymer composites can be prepared as films by blade coating or as bulk samples by techniques such as hot pressing. Methods for characterizing the TE properties of films with small areas ($\approx 5.0 \times 0.104$ mm, 0.1 mm^2)[10,115,116] and small samples (nanowires with an average diameter of 100 nm, needle-shaped samples with dimensions of approximately $0.1 \times 0.05 \times 2$–3 mm)[117–119] can be found in the literature. However, some of these techniques require complicated and labor-intensive sample preparation, such as on-chip heaters.[119] In measurements of α and σ, thin films can be clamped vertically where ΔT is developed along the length of the substrate and film, with the surface of the film facing the inner probes. The film should be of uniform thickness and width so that an accurate cross-sectional area can be calculated. Furthermore, the selected substrate should have low σ to ensure that current passes through the film, and low κ to prevent a thermal short. While the inner probes are in direct contact with the film, the contact of the outer electrodes to the film can be improved by applying silver electrodes on the two ends of the substrate; these added contacts may change the effective length of the sample being tested, but have no bearing on the measured values, as only the distance between the inner probes is important. Notably, electrical measurements are conducted along the length of the film and can vary from values obtained along the thickness or the bulk because of anisotropy. It is generally advisable, and time-saving, to check the resistance of a film with a basic multi-meter and pin-probes at room temperature before loading it into the instrument to verify that the film is continuous throughout the full length and that resistivity is reasonably low to satisfy instrumentation limits.

The substrates for samples used to measure thermal conductivity are different from those needed for measurements of α and σ: to measure κ, substrates with high thermal conductivity are needed. Thus, processing the same quality of films on substrates with widely different thermal properties is important to get meaningful values of σ, α, and κ (and ZT). The thermal diffusivity of the substrate controls the lower thickness limit of the film for such measurements. We note that techniques such as AC-calorimetry or 3ω technique are optimal for thin films, in contrast to thermal-diffusivity measurements.

4. Conclusions and Outlook

The performance of polymers and polymer composites for TE applications can be improved by addressing materials design, composite formation, composite characterization, and ultimately device preparation and characterization (Figure 8). Most examples of polymer composites for TE applications utilize a conjugated polymer matrix, such as PEDOT or PANI, with inorganic or organic fillers. The low thermal

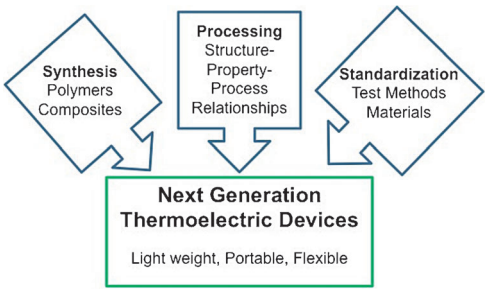

Figure 8. Preparation of next-generation lightweight, portable, and flexible TE devices based on organic polymer composites accessed by combing synthesis, processing, and standardized characterization.

conductivity of organic polymers is reinforced by matrix-filler interface nanostructuring, which help improve the *ZT*. Moreover, organization of polymer chains by crystallization as a result of intermolecular interactions (e.g., π-stacking) or nucleation on the particle surface can enhance σ. As such, the identity of nanoparticle ligands can influence the dispersion of nanoparticles in a matrix and the particle–polymer interactions. The Ag and Au nanoparticle/ligand environment can be tailored using thiol-based ligands,[74,75,120] while functionalization of metal chalcogenides, inorganic materials with the highest TE performance, remain underdeveloped,[61] and techniques for functionalization of carbon nanomaterials have yet to be applied in the context of improved TE properties.[121,122] Ongoing efforts to improve the TE properties of conjugated polymers,[123,124] and the development of new materials will greatly benefit from a thorough understanding of the effects of molecular structure, counterions, dopants, and impurities (e.g., residual catalysts) on the performance.[37] To date, structure–property relationships are not fully defined for even the best-performing polymer blends (partially dedoped PEDOT:PSS) and no systematic study of the TE properties of polymer nanocomposites have been reported. As this field is in its early stages, increased research attention is bound to provide rapid improvements in the development of improved polymer-based systems as TE materials.

The behavior of TE composites depends on the properties of the constituents and the interface between them. If both polymer and nanoparticle are active TE materials, opposite or identical effects on α and σ can be realized, and both components being n-type or p-type is desirable. Moreover, if both are TE materials, good charge transfer between them is necessary and the electronic nature of their interactions must be taken into account, specifically the relative Fermi levels and HOMO–LUMO gaps. An in-depth analysis of charge-carrier transport across interfaces could facilitate the optimization of the TE properties. Alternatively, if only the polymer or particle is a TE material, the active component must percolate the composite for efficient charge transport, and the resistance between the electrically conductive domains must be low.[125] Furthermore, the effects of material's identity and relative particle loadings on α are poorly understood parameters in polymer composites for TE applications, and a better understanding is needed. Some of the best TE composites require CNT loadings much above the percolation threshold for electrical conductivity (>80 wt% vs. 2 wt%),[80,90] and scalable and cost-effective TE composites will only be achieved by optimization at lower loadings.

Improving polymer composites for TE applications will especially benefit from 1) developing n-type materials/composites and 2) decoupling κ, σ, and α to facilitate *ZT* optimization.[126] The vast majority of systems discussed in this review are p-type, which is not surprising given that n-type organic materials are generally unstable under ambient conditions and have a propensity to show ambipolar charge transport.[44,127] Promising n-type organic materials include small-molecule charge-transfer complexes,[128] fullerene-C_{60},[129] and perylene dianhydride.[130] As small molecules have poor mechanical characteristics and the thermal conductivity of crystals is generally higher than that of amorphous materials,[131] a novel opportunity for preparing n-type organic TE materials is the incorporation of molecules in a polymer matrix by blending or covalent attachment to the polymer chain.

Thorough characterization of σ, κ, and α will allow the meaningful measurement of *ZT*, which suggests the usefulness of the material in a TE device, but is no guarantee for it. Comparisons between materials or published reports can only be made with standard characterization techniques. To ensure that measured values are not inflated, the parameters of sample size and shape, identity of substrate and electrode, and sample anisotropy must be reported. Furthermore, TE devices must have balanced *ZT*, σ, and κ between the p-type and n-type legs, and resistance between the active layer and electrode and thermal expansion should be low. Researchers thus have opportunities to explore device design and the lifetime and degradation profile of the materials/devices, especially relevant given the evolution of composite morphology over time.

Polymer-based composites are in the early stages of development for TE applications, and can be compared to organic photovoltaic (OPVs) and light-emitting diodes (OLEDs) just a few decades ago. A promising class of all-organic composites for TE applications is based on carbon nanomaterials in commodity polymers, such as CNTs in PVOAc, which would allow the large-scale preparation of lightweight and flexible TE materials. While *ZT* measurements are important for understanding the properties of the materials, the ultimate usefulness of the materials will be realized by their incorporation into TE generators or Peltier cooling devices with operation temperatures higher than 300 °C, complimentary to inorganic TE materials used at higher temperatures.

We would like to thank J. Mackey and B. Kowalski for help with the table of contents picture. E.B.P. and B.T.M. thank Case Western Reserve University Department of Chemistry and College of Arts And Sciences for financial support; A.S. thanks NASA/USRA contract 04555-004 for financial support.

Received: August 21, 2014
Published online: December 23, 2014

[1] X. Chen, C. Li, M. Grätzel, R. Kostecki, S. S. Mao, *Chem. Soc. Rev.* **2012**, *41*, 7909 – 7937.
[2] X. F. Zheng, C. X. Liu, Y. Y. Yan, Q. Wang, *Renewable Sustainable Energy Rev.* **2014**, *32*, 486 – 503.
[3] H. Bottner, *Mater. Res. Soc. Symp. Proc.* **2009**, *1166*, 1166-N01-01.
[4] O. Bubnova, X. Crispin, *Energy Environ. Sci.* **2012**, *5*, 9345.
[5] Y. Du, S. Z. Shen, K. Cai, P. S. Casey, *Prog. Polym. Sci.* **2012**, *37*, 820 – 841.
[6] M. He, F. Qiu, Z. Lin, *Energy Environ. Sci.* **2013**, *6*, 1352.
[7] D. Crane, J. LaGrandeur, V. Jovovic, M. Ranalli, M. Adldinger, E. Poliquin, J. Dean, D. Kossakovski, B. Mazar, C. Maranville, *J. Electron. Mater.* **2013**, *42*, 1582 – 1591.
[8] J. Martin, T. Tritt, C. Uher, *J. Appl. Phys.* **2010**, *108*, 121101.
[9] *CRC Handbook of Thermoelectrics* (Ed.: T. M. Tritt), CRC, Boca Raton, **2005**.
[10] T. C. Harman, P. J. Taylor, M. P. Walsh, B. E. LaForge, *Science* **2002**, *297*, 2229 – 2232.
[11] R. Venkatasubramanian, E. Siivola, T. Colpitts, B. O'Quinn, *Nature* **2001**, *413*, 597 – 602.
[12] S. J. Thiagarajan, W. Wang, R. Yang, *Annu. Rev. Nano Res.* **2010**, *3*, 555.
[13] K. Nielsch, J. Bachmann, J. Kimling, H. Böttner, *Adv. Energy Mater.* **2011**, *1*, 713 – 731.
[14] F. W. Dynys, M.-H. Berger, A. Sehirlioglu, *J. Am. Ceram. Soc.* **2012**, *95*, 619 – 626.
[15] F. W. Dynys, A. Sayir, J. Mackey, A. Sehirlioglu, *J. Alloys Compd.* **2014**, *604*, 196 – 203.
[16] A. Nag, V. Shubha, *J. Electron. Mater.* **2014**, *43*, 962 – 977.
[17] S. Walia, S. Balendhran, H. Nili, S. Zhuiykov, G. Rosengarten, Q. H. Wang, M. Bhaskaran, S. Sriram, M. S. Strano, K. Kalantar-zadeh, *Prog. Mater. Sci.* **2013**, *58*, 1443 – 1489.
[18] N. N. Van, N. Pryds, *Adv. Nat. Sci. Nanosci. Nanotechnol.* **2013**, *4*, 023002.
[19] M. O'Neill, S. M. Kelly, *Adv. Mater.* **2011**, *23*, 566 – 584.
[20] E. Moulin, J.-J. Cid, N. Giuseppone, *Adv. Mater.* **2013**, *25*, 477 – 487.
[21] X. Guo, M. Baumgarten, K. Müllen, *Prog. Polym. Sci.* **2013**, *38*, 1832 – 1908.
[22] D. Angmo, S. a. Gevorgyan, T. T. Larsen-Olsen, R. R. Søndergaard, M. Hösel, M. Jørgensen, R. Gupta, G. U. Kulkarni, F. C. Krebs, *Org. Electron.* **2013**, *14*, 984 – 994.
[23] A. B. Kaiser, *Rep. Prog. Phys.* **2001**, *64*, 1 – 49.
[24] T. Emrick, E. Pentzer, *NPG Asia Mater.* **2013**, *5*, e43.
[25] T. O. Poehler, H. E. Katz, *Energy Environ. Sci.* **2012**, *5*, 8110 – 8115.
[26] D. Zhao, G. Tan, *Appl. Therm. Eng.* **2014**, *66*, 15 – 24.
[27] *Handbook of Advanced Electronic and Photonic Materials and Devices* (Ed.: F. Mohammad), Academic Press, **2001**, pp. 321 – 350.
[28] H. Kaneko, T. Ishiguro, A. Takahashi, J. Tsukamoto, *Synth. Met.* **1993**, *57*, 4900 – 4905.
[29] N. Mateeva, H. Niculescu, J. Schlenoff, L. R. Testardi, *J. Appl. Phys.* **1998**, *83*, 3111.
[30] C. O. Yoon, M. Reghu, D. Moses, Y. Cao, A. J. Heeger, *Synth. Met.* **1995**, *69*, 255 – 258.
[31] N. T. Kemp, A. B. Kaiser, C. Liu, B. Chapman, O. Mercier, A. M. Carr, H. J. Trodahl, R. G. Buckley, A. C. Partridge, J. Y. Lee, et al., *J. Polym. Sci. Part B* **1998**, *37*, 953 – 960.
[32] S. Wakim, B. Aïch, Y. Tao, M. Leclerc, *Polym. Rev.* **2008**, *48*, 432 – 462.
[33] B. Aïch, N. Blouin, A. Bouchard, M. Leclerc, *Chem. Mater.* **2009**, *21*, 751 – 757.
[34] Y. Hu, H. Shi, H. Song, C. Liu, J. Xu, L. Zhang, Q. Jiang, *Synth. Met.* **2013**, *181*, 23 – 26.
[35] Y. Hiroshige, M. Ookawa, N. Toshima, *Synth. Met.* **2007**, *157*, 467 – 474.
[36] G.-H. Kim, L. Shao, K. Zhang, K. P. Pipe, *Nat. Mater.* **2013**, *12*, 719 – 723.
[37] O. Bubnova, M. Berggren, X. Crispin, *J. Am. Chem. Soc.* **2012**, *134*, 16456 – 16459.
[38] Q. Jiang, C. Liu, J. Xu, B. Lu, H. Song, H. Shi, Y. Yao, L. Zhang, *J. Polym. Sci. Part B* **2014**, *52*, 737 – 742.
[39] R. Yue, J. Xu, *Synth. Met.* **2012**, *162*, 912 – 917.
[40] O. Bubnova, Z. U. Khan, A. Malti, S. Braun, M. Fahlman, M. Berggren, X. Crispin, *Nat. Mater.* **2011**, *10*, 429 – 433.
[41] Y. Sun, P. Sheng, C. Di, F. Jiao, W. Xu, D. Qiu, D. Zhu, *Adv. Mater.* **2012**, *24*, 932 – 937.
[42] Q. Zhang, Y. Sun, W. Xu, D. Zhu, *Adv. Mater.* **2014**, DOI: 10.1002/adma.201305371.
[43] A. Wagner, H. Kliem, *J. Phys. D.* **2003**, *6*, 343 – 347.
[44] A. Babel, J. D. Wind, S. A. Jenekhe, *Adv. Funct. Mater.* **2004**, *14*, 891 – 898.
[45] T. A. M. Ferenczi, C. Müller, D. D. C. Bradley, P. Smith, J. Nelson, N. Stingelin, *Adv. Mater.* **2011**, *23*, 4093 – 4097.
[46] See Ref. [44].
[47] Y. Kojima, A. Usuki, M. Kawasumi, A. Okada, Y. Fukushima, *J. Mater. Res.* **1993**, *8*, 1185 – 1189.
[48] P. Akcora, H. Liu, S. K. Kumar, J. Moll, Y. Li, B. C. Benicewicz, L. S. Schadler, D. Acehan, A. Z. Panagiotopoulos, V. Pryamitsyn, V. Ganesanet, J. Ilavsky, P. Thiyagarajan, R. H. Colby, J. F. Douglas, *Nat. Mater.* **2009**, *8*, 354 – 359.
[49] R. Chan, R. C. Y. King, F. Roussel, J.-F. Brun, C. Gors, *Synth. Met.* **2012**, *162*, 1348 – 1356.
[50] O. Bubnova, Z. U. Khan, H. Wang, S. Braun, D. R. Evans, M. Fabretto, P. Hojati-Talemi, D. Dagnelund, J.-B. Arlin, Y. H. Geerts, S. Desbief, D. W. Breiby, J. W. Andreasen, R. Lazzaroni, W. M. Chen, I. Zozoulenko, M. Fahlman, P. J. Murphy, M. Berggren, X. Crispin, *Nat. Mater.* **2014**, *13*, 190 – 194.
[51] A. Ueda, Y. Omura, S. Nagai, *Polymer* **1997**, *38*, 801 – 807.
[52] P. J. Brigandi, J. M. Cogen, R. A. Pearson, *Polym. Eng. Sci.* **2014**, *54*, 1 – 16.
[53] K. Fehse, K. Walzer, K. Leo, W. Lövenich, A. Elschner, *Adv. Mater.* **2007**, *19*, 441 – 444.
[54] V. Jousseaume, M. Morsli, A. Bonnet, O. Tesson, S. Lefrant, *J. Appl. Polym. Sci.* **1998**, *67*, 1205 – 1208.
[55] C. Y. Yang, Y. Cao, P. Smith, A. J. Heeger, *Synth. Met.* **1993**, *53*, 293 – 301.
[56] J. Sun, M.-L. Yeh, B. J. Jung, B. Zhang, J. Feser, A. Majumdar, H. E. Katz, *Macromolecules* **2010**, *43*, 2897 – 2903.
[57] X. Gao, K. Uehara, D. Klug, S. Patchkovskii, J. Tse, T. Tritt, *Phys. Rev. B* **2005**, *72*, 125202.
[58] R. Schlitz, F. G. Brunetti, A. M. Glaudell, P. L. Miller, M. Brady, C. J. Takacs, C. J. Hawker, M. L. Chabinyc, *Adv. Mater.* **2014**, *26*, 2825 – 2830.
[59] Y. Wang, K. Cai, X. Yao, *ACS Appl. Mater. Interfaces* **2011**, *3*, 1163 – 1166.
[60] L. M. Goncalves, C. Couto, P. Alpuim, A. G. Rolo, F. Völklein, J. H. Correia, *Thin Solid Films* **2010**, *518*, 2816 – 2821.
[61] K. C. See, J. P. Feser, C. E. Chen, A. Majumdar, J. J. Urban, R. Segalman, *Nano Lett.* **2010**, *10*, 4664 – 4667.
[62] N. E. Coates, S. K. Yee, B. McCulloch, K. C. See, A. Majumdar, R. A. Segalman, J. J. Urban, *Adv. Mater.* **2013**, *25*, 1629 – 1633.
[63] K. Chatterjee, M. Mitra, K. Kargupta, S. Ganguly, D. Banerjee, *Nanotechnology* **2013**, *24*, 215703.
[64] Y. Du, K. F. Cai, S. Chen, P. Cizek, T. Lin, *ACS Appl. Mater. Interfaces* **2014**, *6*, 5753 – 5743.
[65] B. Zhang, J. Sun, H. E. Katz, F. Fang, R. L. Opila, *ACS Appl. Mater. Interfaces* **2010**, *2*, 3170 – 3178.
[66] J. N. Coleman, M. Lotya, A. O'Neill, S. D. Bergin, P. J. King, U. Khan, K. Young, A. Gaucher, S. De, R. J. Smith, et al., *Science* **2011**, *331*, 568 – 571.

[67] M. Buscema, M. Barkelid, V. Zwiller, H. S. J. van der Zant, G. Steele, A. Castellanos-Gomez, *Nano Lett.* **2013**, *13*, 358 – 363.
[68] X.-Z. Guo, Y.-D. Zhang, D. Qin, Y.-H. Luo, D.-M. Li, Y.-T. Pang, Q.-B. Meng, *J. Power Sources* **2010**, *195*, 7684 – 7690.
[69] A. V. Murugan, M. Quintin, M.-H. Delville, G. Campet, A. K. Viswanath, C. S. Gopinath, K. Vijayamohanan, *J. Mater. Res.* **2006**, *21*, 112 – 118.
[70] M. G. Kanatzidis, R. Bissessur, D. C. DeGroot, J. L. Schindler, C. R. Kannewurf, M. S. Uniuersity, C. Science, *Chem. Mater.* **1993**, *5*, 595 – 596.
[71] L. Wang, J. Schindler, J. A. Thomas, C. R. Kannewurf, M. G. Kanatzidis, *Chem. Mater.* **1995**, *7*, 1753 – 1755.
[72] R. Bissessur, M. G. Kanatzidis, J. L. Schindler, C. R. Kannewurf, C. R. Kannewurf, *Chem. Commun.* **1993**, 1582 – 1585.
[73] L. Schindler, C. R. Kannewurk, M. Kanatzidis, *Mol. Cryst. Liq. Cryst. Sci. Technol. Sect. A* **1994**, *245*, 249 – 254.
[74] E. Pinter, Z. A. Fekete, O. Berkesi, P. Makra, A. Patzko, C. Visy, *J. Phys. Chem. C* **2007**, *111*, 11872 – 11878.
[75] N. Toshima, N. Jiravanichanun, H. Marutani, *J. Electron. Mater.* **2012**, *41*, 1735 – 1742.
[76] T. Ramanathan, A. A. Abdala, S. Stankovich, D. Dikin, M. Herrera-Alonso, R. D. Piner, D. H. Adamson, H. C. Schniepp, X. Chen, R. S. Ruoff, S. T. Nguyen, I. A. Aksay, R. K. Prud'homme, L. C. Brinson, *Nat. Nanotechnol.* **2008**, *3*, 327 – 331.
[77] Z. Sun, D. K. James, J. M. Tour, *J. Phys. Chem. Lett.* **2011**, *2*, 2425 – 2432.
[78] M. Piao, J. Na, J. Choi, J. Kim, G. P. Kennedy, G. Kim, S. Roth, U. Dettlaff-Weglikowska, *Carbon* **2013**, *62*, 430 – 437.
[79] D. Kim, Y. Kim, K. Choi, J. C. Grunlan, C. Yu, *ACS Nano* **2010**, *4*, 513 – 523.
[80] G. P. Moriarty, S. De, P. J. King, U. Khan, M. Via, J. A. King, J. N. Coleman, J. C. Grunlan, *J. Polym. Sci. Part B* **2013**, *51*, 119 – 123.
[81] C. Yu, K. Choi, L. Yin, J. C. Grunlan, *ACS Nano* **2011**, *5*, 7885 – 7892.
[82] K. Zhang, M. Davis, J. Qiu, L. Hope-Weeks, S. Wang, *Nanotechnology* **2012**, *23*, 385701.
[83] B. Abad, I. Alda, P. Díaz-Chao, H. Kawakami, A. Almarza, D. Amantia, D. Gutierrez, L. Aubouy, M. Martín-González, *J. Mater. Chem. A* **2013**, *1*, 10450 – 10457.
[84] C. Yu, Y. S. Kim, D. Kim, J. C. Grunlan, *Nano Lett.* **2008**, *8*, 4428 – 4432.
[85] Y. Zhao, G.-S. Tang, Z.-Z. Yu, J.-S. Qi, *Carbon* **2012**, *50*, 3064 – 3073.
[86] S. Amemori, K. Kokado, K. Sada, *Angew. Chem. Int. Ed.* **2013**, *52*, 4174 – 4178.
[87] N. Liu, Z. Chen, D. R. Dunphy, Y.-B. Jiang, R. Assink, C. J. Brinker, *Angew. Chem. Int. Ed.* **2003**, *42*, 1731 – 1734; *Angew. Chem.* **2003**, *115*, 1773 – 1776.
[88] G. P. Moriarty, J. N. Wheeler, C. Yu, J. C. Grunlan, *Carbon* **2012**, *50*, 885 – 895.
[89] D. D. Freeman, K. Choi, C. Yu, *PLoS One* **2012**, *7*, e47822.
[90] C. Hewitt, A. B. Kaiser, S. Roth, M. Craps, R. Czerw, D. L. Carroll, *Nano Lett.* **2012**, *12*, 1307 – 1310.
[91] C. Hewitt, A. B. Kaiser, M. Craps, R. Czerw, S. Roth, D. L. Carrol, *Synth. Met.* **2013**, *165*, 56 – 59.
[92] H. Wang, W. D. Porter, H. Böttner, J. König, L. Chen, S. Bai, T. M. Tritt, A. Mayolet, J. Senawiratne, C. Smith, F. Harris, P. Gilbert, J. W. Sharp, J. Lo, H. Kleinke, L. Kiss, *J. Electron. Mater.* **2013**, *42*, 654 – 664.
[93] N. D. Lowhorn, W. Wong-Ng, Z.-Q. Lu, J. Martin, M. L. Green, J. E. Bonevich, E. L. Thomas, N. R. Dilley, J. Sharp, *J. Mater. Res.* **2011**, *26*, 1983 – 1992.
[94] J. Snyder, B. B. Iversen, K. Borup, E. Mueller, J. de Boor, L. Chen, X. Shi, F. Gascoin, H. Wang, M. Fedorov, *Energy Environ. Sci.*, **2014**, DOI: 10.1039/C4EE01320D.
[95] See Ref. [7]
[96] J. Mackey, A. Sehirlioglu, F. Dynys, *Appl. Energy* **2014**, *134*, 374 – 381.
[97] F. Chen, J. C. Cooley, W. L. Hults, J. L. Smith, *Rev. Sci. Instrum.* **2001**, *72*, 4201 – 4206.
[98] W. H. Kettler, R. Weinhart, M. Rosenberg, *Rev. Sci. Instrum.* **1986**, *57*, 3053 – 3058.
[99] G. Min, D. M. Rowe, *Meas. Sci. Technol.* **2001**, *12*, 1261 – 1262.
[100] J. de Boor, E. Müller, *Rev. Sci. Instrum.* **2013**, *84*, 065102.
[101] S. Iwanaga, E. S. Toberer, A. LaLonde, G. J. Snyder, *Rev. Sci. Instrum.* **2011**, *82*, 063905.
[102] C. N. Berglund, R. C. Beairsto, *Rev. Sci. Instrum.* **1967**, *38*, 66 – 68.
[103] J. Martin, *Meas. Sci. Technol.* **2013**, *24*, 085601.
[104] J. Mackey, F. Dynys, A. Sehirlioglu, *Rev. Sci. Instrum.* **2014**, *85*, 085119.
[105] O. Boffoué, A. Jacquot, A. Dauscher, B. Lenoir, M. Stölzer, *Rev. Sci. Instrum.* **2005**, *76*, 053907.
[106] M. Thermitus, P. S. Gaal in *Proc. 24th Int. Therm. Conduct. Conf. Proc. 12th Int. Therm. Exp. Symp.* (Eds.: P. S. Gaal, D. E. Apostolescu), **1997**, 219.
[107] M. Thermitus, P. C. Gaal, in *Proc. 25th Int. Therm. Conduct. Conf. Proc. 13th Int. Therm. Exp. Symp.* (Eds.: C. Uher, D. Morellie), **1999**, p. 340.
[108] P. H. M. Böttger, E. Flage-Larsen, O. B. Karlsen, T. G. Finstad, *Rev. Sci. Instrum.* **2012**, *83*, 025101.
[109] R. Taylor in *CRC Handbook of Thermoelectrics* (Ed.: M. Rowe), CRC Press, Boca Raton, **2005**.
[110] G. K. White in *Thermal Conductivity* (Ed.: R. P. Tye), Academic Press, London, **1969**.
[111] W. J. Parker, R. J. Jenkins, C. P. Butler, G. L. Abbott, *J. Appl. Phys.* **1961**, *32*, 1679.
[112] L. M. Clark III, R. E. Taylor, *J. Appl. Phys.* **1975**, *46*, 714.
[113] R. D. Cowan, *J. Appl. Phys.* **1963**, *34*, 926.
[114] D. E. Stroe, P. S. Gaal, M. A. Thermitus, S. P. Apostolescu, A. Millea, in *Proc. 27th Int. Therm. Cond. Conf. Proc. 15th Int. Therm. Exp. Symp.* (Eds.: H. Wang, W. D. Porter, G. Worley), **2003**, p. 473.
[115] S. Iwanaga, G. J. Snyder, *J. Electron. Mater.* **2012**, *41*, 1667 – 1674.
[116] W. M. N. W. Jaafar, J. E. Snyder, G. Min, *Rev. Sci. Instrum.* **2013**, *84*, 054903.
[117] T. Dasgupta, A. M. Umarji, *Rev. Sci. Instrum.* **2005**, *76*, 094901.
[118] A. L. Pope, R. T. Littleton, T. M. Tritt, *Rev. Sci. Instrum.* **2001**, *72*, 3129.
[119] A. I. Hochbaum, R. Chen, R. D. Delgado, W. Liang, E. C. Garnett, M. Najarian, A. Majumdar, P. Yang, *Nature* **2008**, *451*, 163 – 167.
[120] B. J. Kim, J. Bang, C. J. Hawker, E. J. Kramer, *Macromolecules* **2006**, *39*, 4108 – 4114.
[121] D. Tasis, N. Tagmatarchis, A. Bianco, M. Prato, *Chem. Rev.* **2006**, *106*, 1105 – 1136.
[122] B. T. McGrail, B. J. Rodier, E. Pentzer, *Chem. Mater.* **2014**, *26*, 5906 – 5811.
[123] M.-C. Ho, C.-H. Chao, A.-Y. Lo, C.-H. Chen, R.-J. Wu, M.-H. Tsai, Y.-C. Huang, W.-T. Whanga, *Mater. Chem. Phys.* **2013**, *141*, 920 – 928.
[124] S. Wei, J. Xia, E. J. Dell, Y. Jiang, R. Song, H. Lee, P. Rodenbough, A. L. Briseno, L. M. Campos, *Angew. Chem. Int. Ed.* **2014**, *53*, 1832 – 1836; *Angew. Chem.* **2014**, *126*, 1863 – 1867.
[125] L. Wang, Q. Yao, H. Bi, F. Huang, Q. Wanga, L. Chen, *J. Mater. Chem. A* **2014**, *2*, 11107.
[126] B. Russ, M. J. Robb, F. G. Brunetti, P. L. Miller, E. E. Perry, S. N. Patel, V. Ho, W. B. Chang, J. J. Urban, M. L. Chabinyc, C. J. Hawker, R. A. Segalman, *Adv. Mater.* **2014**, *26*, 3473 – 3477.

[127] J. E. Anthony, A. Facchetti, M. Heeney, S. R. Marder, X. Zhan, *Adv. Mater.* **2010**, *22*, 3876 – 3892.
[128] H. Itahara, M. Maesato, R. Asahi, H. Yamochi, G. Saito, *J. Electron. Mater.* **2009**, *38*, 1171 – 1175.
[129] M. Sumino, K. Harada, M. Ikeda, S. Tanaka, K. Miyazaki, C. Adachi, *Appl. Phys. Lett.* **2011**, *99*, 093308.
[130] J. Wuesten, C. Ziegler, T. Ertl, *Phys. Rev. B* **2006**, *74*, 125205.
[131] X. Huang, M. Roushan, T. J. Emge, W. Bi, S. Thiagarajan, J.-H. Cheng, R. Yang, J. Li, *Angew. Chem. Int. Ed.* **2009**, *48*, 7871 – 7874; *Angew. Chem.* **2009**, *121*, 8011 – 8014.

